

## GENERAL RELATIVISTIC INSTABILITY SUPERNOVA OF A SUPERMASSIVE POPULATION III STAR

KE-JUNG CHEN<sup>1,2,\*</sup>, ALEXANDER HEGER<sup>3</sup>, S. E. WOOSLEY<sup>1</sup>, ANN ALMGREN<sup>4</sup>, DANIEL J. WHALEN<sup>5,6</sup>, AND JARRETT L. JOHNSON<sup>7</sup>*Draft version February 20, 2014*

## ABSTRACT

The formation of supermassive Population III stars with masses  $\gtrsim 10,000 M_{\odot}$  in primeval galaxies in strong UV backgrounds at  $z \sim 15$  may be the most viable pathway to the formation of supermassive black holes by  $z \sim 7$ . Most of these stars are expected to live for short times and then directly collapse to black holes, with little or no mass loss over their lives. But we have now discovered that non-rotating primordial stars with masses close to  $55,000 M_{\odot}$  can instead die as highly energetic thermonuclear supernovae powered by explosive helium burning, releasing up to  $10^{55}$  erg, or about 10,000 times the energy of a Type Ia supernova. The explosion is triggered by the general relativistic contribution of thermal photons to gravity in the core of the star, which causes the core to contract and explosively burn. The energy release completely unbinds the star, leaving no compact remnant, and about half of the mass of the star is ejected into the early cosmos in the form of heavy elements. The explosion would be visible in the near infrared at  $z \lesssim 20$  to *Euclid* and the Wide-Field Infrared Survey Telescope (WFIRST), perhaps signaling the birth of supermassive black hole seeds and the first quasars.

*Subject headings:* cosmology: early universe - theory - galaxies: formation - hydrodynamics - galaxies: high-redshift - stars: early-type - supernovae: general - shocks - quasars: supermassive black holes

## 1. INTRODUCTION

The existence of supermassive black holes (SMBHs) in most massive galaxies today poses significant challenges to the paradigm of hierarchical structure formation (Kormendy & Richstone 1995; Ferrarese & Merritt 2000; Ferrarese & Ford 2005; Gebhardt et al. 2000; Di Matteo et al. 2005; Beifiori et al. 2012; McConnell & Ma 2013). In particular, it is not known how some SMBHs reached masses of  $10^9 M_{\odot}$  by  $z \sim 7$ , less than a Gyr after the big bang (Fan et al. 2002, 2006; Mortlock et al. 2011). The two leading contenders for the origins of SMBHs are 100 - 500  $M_{\odot}$  Population III (Pop III) stars at  $z \sim 20$  and supermassive ( $10^4$  -  $10^5 M_{\odot}$ ) Pop III stars at  $z \sim 10$  - 15 (e.g., Rees 1984; Madau & Rees 2001; Volonteri 2010, 2012; Karlsson et al. 2013).

The main argument against conventional Pop III stars as SMBH seeds is that their BHs must accrete at the Eddington limit continuously down to  $z \sim 7$  to become supermassive. How they could sustain such growth is unclear because they form in low-density relic H II regions that delay initial accretion (Whalen et al. 2004; Johnson

& Bromm 2007). Later, when they do accrete, the relatively shallow dark matter potential wells in which they reside cannot retain their fuel supply because of radiative feedback (Alvarez et al. 2009), so they grow at well below the Eddington limit (Park & Ricotti 2011, 2012, 2013). Furthermore, many low-mass Pop III black holes are ejected from their halos (and thus their fuel supply) at birth by asymmetries in their explosion engines (Whalen & Fryer 2012).

For these reasons, there has been growing interest in supermassive stars (SMSs) as candidates for SMBH seeds (e.g., Loeb & Rasio 1994; Bromm & Loeb 2003; Begelman et al. 2006; Bromm & Yoshida 2011; Johnson et al. 2013c). Such stars could form in atomically-cooled halos at  $z \sim 15$ . In this scenario, a primeval galaxy forms in a strong Lyman-Werner (LW) UV background that sterilizes its constituent halos of H<sub>2</sub> prior to assembly (Agarwal et al. 2012; Johnson et al. 2013a), preventing them from forming stars. When the protogalaxy reaches a mass of  $\sim 10^8 M_{\odot}$  and virial temperature of  $\sim 10^4$  K, atomic cooling triggers the rapid collapse of gas at its center at rates of up to  $1 M_{\odot} \text{ yr}^{-1}$  (Lodato & Natarajan 2006; Spaans & Silk 2006; Wise et al. 2008; Regan & Haehnelt 2009; Shang et al. 2010; Latif et al. 2013a,b; Schleicher et al. 2013). In this manner, a  $10^4$  -  $10^5 M_{\odot}$  Pop III star could be formed in less than a Myr.

The evolution of supermassive protostars and stars has been studied with both analytical and numerical techniques for over 40 years (Fowler 1966; Wheeler 1977; Bond et al. 1984; Carr et al. 1984; Fuller et al. 1986; Bisnovatyi-Kogan 1998; Baumgarte & Shapiro 1999; Begelman 2010; Hosokawa et al. 2013; Schleicher et al. 2013). Most SMSs are thought to become fully convective and then later collapse to massive BHs (e.g., Shapiro & Teukolsky 1979; Shibata & Shapiro 2002; Reisswig

\* IAU Gruber Fellow; kchen@ucolick.org

<sup>1</sup> Department of Astronomy & Astrophysics, University of California, Santa Cruz, CA 95064, USA

<sup>2</sup> School of Physics and Astronomy, University of Minnesota, Minneapolis, MN 55455, USA

<sup>3</sup> Monash Centre for Astrophysics, Monash University, Victoria 3800, Australia

<sup>4</sup> Center for Computational Sciences and Engineering, Lawrence Berkeley National Lab, Berkeley, CA 94720, USA

<sup>5</sup> T-2, Los Alamos National Laboratory, Los Alamos, NM 87545, USA

<sup>6</sup> Universität Heidelberg, Zentrum für Astronomie, Institut für Theoretische Astrophysik, Albert-Ueberle-Str. 2, 69120 Heidelberg, Germany

<sup>7</sup> XTD-PRI, Los Alamos National Laboratory, Los Alamos, NM 87545, USA

et al. 2013). However, previous calculations of SMS evolution have been done at low resolution, considered a relatively coarse grid of models in mass, and in some cases ignored first-order, post-Newtonian general relativistic corrections to gravity. The latter could play an important role in the evolution of  $10^3 - 10^5 M_\odot$  stars, especially during their pre-explosion phase.

We have revisited the evolution of Pop III SMSs with high-resolution one-dimensional (1D) simulations with updated nuclear reaction rates (Heger et al. 2001; Heger & Woosley 2002) and post-Newtonian corrections to gravity. We have found a  $55,500 M_\odot$  star that explodes as a highly energetic thermonuclear supernova (SN) instead of collapsing to a BH (see also Montero et al. 2012). Our discovery suggests that there may be a range of high-mass stars that can die as SNe. In Section 2 we describe our stellar evolution model. The explosion of the star is examined in 1D in Section 3 and in two dimensions (2D) in Section 4. We discuss the potential impact of this explosion on its host galaxy and its visibility at high redshift in Section 5.

## 2. NUMERICAL MODEL

The SMS is evolved from the beginning of the main sequence to the onset of collapse and then explosion in 1D in **KEPLER**. To verify these processes in a separate code, and to capture the violent fluid instabilities that can occur during the SN, we also model the collapse and explosion of the SMS in 2D in **CASTRO** with initial conditions taken from **KEPLER**. Combining 1D and 2D simulations in this manner allows us to realistically simulate all phases of the SMS within a practical computational budget.

### 2.1. **KEPLER**

**KEPLER** (Weaver et al. 1978) is a 1D Lagrangian hydrodynamics and stellar evolution code. It includes nuclear burning and mixing due to convection. For a given stellar mass, the initial profiles of density and temperature of a star are determined by solving the Lane-Emden equation (Chandrasekhar 1939). We use the 19-isotope APPROX nuclear reaction network (Weaver et al. 1978; Timmes 1999), which includes heavy-ion reactions, alpha-chain reactions, hydrogen burning cycles, photo-disintegration of heavy nuclei, and energy loss through thermal neutrinos. Nuclear burning is self-consistently coupled to hydrodynamics, and we also account for energy deposition due to radioactive decay of  $^{56}\text{Ni} \rightarrow ^{56}\text{Co} \rightarrow ^{56}\text{Fe}$ . **KEPLER** uses the Helmholtz equation of state (EOS; Timmes & Swesty 2000), which includes contributions from degenerate and non-degenerate relativistic and non-relativistic electrons, electron-positron pair production, and radiation. The star is partitioned into 1201 zones in mass for an effective resolution of  $46.2 M_\odot$ . Consistent with the usual convention that massive Pop III stars lose little of their mass over their lives (Kudritzki 2000; Vink et al. 2001; Baraffe et al. 2001; Krücka & Kubát 2006; Ekström et al. 2008), we turn off mass loss in our models.

When stars become extremely massive,  $\gtrsim 1000 M_\odot$ , general relativity (GR) must be taken into account in gravity in stellar evolution models. Instead of full GR, we apply first-order post-Newtonian GR corrections to gravity in our calculations. We use the Tolman-Oppenheimer-Volkoff equation for hydrostatic equilibrium in GR to calculate the pressure  $P$  (Zeldovich &

Novikov 1971; Kippenhahn & Weigert 1990):

$$\frac{dP}{dr} = -\frac{Gm}{r^2} \varrho \left(1 + \frac{P}{\varrho c^2}\right) \left(1 + \frac{4\pi r^3 P}{mc^2}\right) \left(1 - \frac{2Gm}{rc^2}\right)^{-1}, \quad (1)$$

where  $r$  is the radius of star,  $c$  is the speed of light,  $G$  is the gravitational constant, and  $m$  is the enclosed relativistic mass at  $r$ , which is the rest mass plus total energy (internal plus gravitational) divided by  $c^2$ . The relativistic density  $\varrho$  is therefore  $\varrho_0 + U/c^2$ , where  $\varrho_0$  and  $U$  are the rest-mass and total energy densities. When  $c^2 \rightarrow \infty$ , Equation (1) reduces to Newton's Law,

$$\frac{dP}{dr} = -\frac{Gm}{r^2} \varrho. \quad (2)$$

The effective gravity  $\tilde{g}$  is calculated from

$$\tilde{g} = -\frac{Gm}{r^2} \left(1 + \frac{P}{\varrho c^2}\right) \left(1 + \frac{4\pi r^3 P}{mc^2}\right) \left(1 - \frac{2Gm}{rc^2}\right)^{-1}. \quad (3)$$

The  $U/c^2$  term in  $\varrho$  is negligible in our models. It only becomes comparable to the rest energy when  $T$  becomes  $\sim 10^{13}$  K ( $kT \sim m_p c^2$ , where  $m_p$  is the proton mass). Equation (3) therefore becomes

$$\tilde{g} = g \left(1 + \frac{P}{\varrho_0 c^2} + \frac{4\pi r^3 P}{mc^2} + \frac{2Gm}{rc^2}\right), \quad (4)$$

where  $g$  is the Newtonian gravity field, which is determined from the gravity equation in **KEPLER** and from the monopole approximation to gravity for nearly spherical matter distributions in **CASTRO**.

### 2.2. **CASTRO**

**CASTRO** is a multidimensional adaptive mesh refinement (AMR) hydrodynamics code. It has a second-order unsplit Godunov hydro scheme and block-structured AMR (Almgren et al. 2010; Zhang et al. 2011). We use the same Helmholtz EOS, APPROX reaction network, energy deposition due to  $^{56}\text{Ni}$  and GR corrections to pressure and gravity in **CASTRO** as in **KEPLER**. As in **KEPLER**, this reaction network is sufficient to capture the key nucleosynthetic pathways and energetics of SMS evolution and explosion. **CASTRO** evolves mass fractions for each isotope with its own advection equation. The monopole approximation is used for self-gravity, in which a 1D gravitational potential is constructed from the radial average of the density and then applied to gravitational force updates everywhere in the AMR hierarchy. This approximation is well-suited to the nearly spherical symmetry of the star and is quite efficient.

We port the star from **KEPLER** onto a 2D cylindrical coordinate grid in  $r$  and  $z$  in **CASTRO** with the conservative mapping scheme of Chen et al. (2013). This is done at the onset of collapse, 600 seconds before the core of the star reaches maximum compression and the most violent burning begins. We simulate the half star in 2D, so the mesh is  $2 \times 10^{13}$  cm in  $r$  and  $4 \times 10^{13}$  cm in  $z$ , which just accommodates the entire star. The coarse grid has 256 zones in  $r$  and 512 zones in  $z$ , with up to two levels of AMR refinement for an additional factor of up to 16 in resolution. The inner core, where most of the explosive burning occurs, is always at the highest resolution; additional criteria for mesh refinement depend on gradients of the density, velocity, and pressure. The highest

spatial resolution of our simulation is about  $5 \times 10^9$  cm to resolve the length scale of nuclear burning. Reflecting and outflow boundary conditions are set on the inner and outer boundaries in both  $r$  and  $z$ , respectively. The simulation is halted when the SN ejecta become frozen in mass coordinates (homologous expansion).

### 3. THE 1D KEPLER EXPLOSION

The SMS has a radius of  $1.73 \times 10^{13}$  cm, an effective surface temperature of about  $7.19 \times 10^4$  K, and a luminosity of  $5.70 \times 10^{42}$  erg sec $^{-1}$  during its pre-collapse phase. The star evolves about 1.69 Myr before beginning to collapse. When it begins helium burning, the central density and temperature are  $\sim 10$  g cm $^{-3}$  and  $2.0 \times 10^8$  K, respectively. Radiation dominates the pressure in the core, and the adiabatic index,  $\gamma_{ad}$ , is slightly above  $4/3$ . At this density and temperature, even the most energetic photons in the Maxwellian distribution cannot create electron-positron pairs and cause  $\gamma_{ad}$  to fall below  $4/3$ . Pair production therefore does not trigger collapse in the SMS. Instead, the energy density of the thermal photons in the high temperature and very low density of the core begins to affect the gravitational field by contributing to the source term in Einstein's field equation, in effect becoming an additional source of gravity. The ratio of the radiative pressure to the relativistic density  $P/(\rho c^2)$  becomes  $\sim 1.3 \times 10^{-3}$ . This causes  $\gamma_{ad}$  in the core to fall below  $4/3$ , and it begins to contract.

Although the temperature and density in the core now rise rapidly and accelerate nuclear burning, they are not high enough to ignite carbon burning, which is the next stage after helium burning. Helium instead begins to burn explosively in the core, burning to carbon first through the triple  $\alpha$  reaction and then to  $^{16}\text{O}$ ,  $^{20}\text{Ne}$ ,  $^{24}\text{Mg}$  and  $^{28}\text{Si}$  through  $\alpha$  capture reactions. These reactions release enough energy to reverse collapse. We show the evolution of radial velocities in the star in Figure 1. The onset and reversal of collapse is evident, together with the formation of the outgoing shock, which propagates outward at several thousand kilometers per second. The shock breaks through the surface of the star 11,880 seconds after core bounce.

The binding energy of the star prior to collapse is  $5.76 \times 10^{53}$  erg, but explosive helium burning releases  $6.52 \times 10^{54}$  erg. We show the evolution of density and temperature at the center of the star in Figure 2. They are initially  $\sim 20$  g cm $^{-3}$  and  $3.6 \times 10^8$  K, and then rise to peak values of  $360$  g cm $^{-3}$  and  $8.26 \times 10^8$  K at core bounce before beginning to fall. The relative magnitudes of the binding and explosion energies together with the rapidly falling density at the center of the star strongly suggest that the SN completely unbinds the star, with no BH formation.

### 4. THE 2D CASTRO EXPLOSION

We initialize CASTRO with the KEPLER profile of the collapsing star 600 seconds prior to maximum core compression. In the beginning of the CASTRO run, the core temperature  $T_c$  and density  $\rho_c$  are  $8.21 \times 10^8$  K and  $356$  g cm $^{-3}$ , respectively. Element masses as a function of radius are shown in Figure 3. The mass of the helium core is  $\sim 31,000 M_\odot$ , and it also contains  $^{28}\text{Si}$ ,  $^{24}\text{Mg}$ ,  $^{20}\text{Ne}$ ,  $^{16}\text{O}$  and  $^{12}\text{C}$ . As in KEPLER, the collapse is reversed by nuclear energy release, but violent fluid

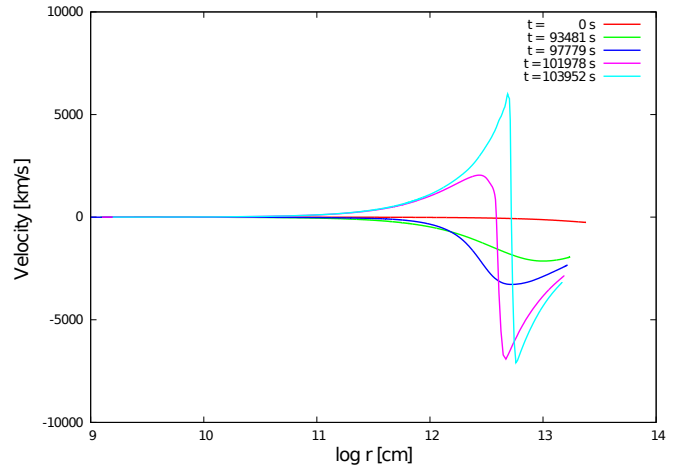


FIG. 1.— Radial velocities in the star from the onset of collapse to explosion. Infall during collapse reaches velocities above  $7000$  km sec $^{-1}$ .

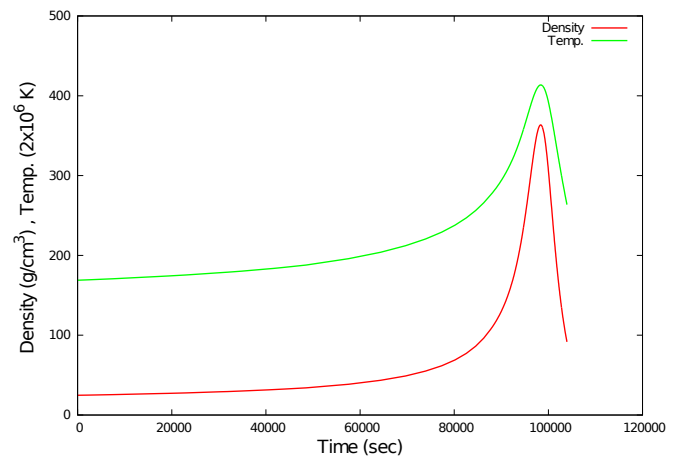


FIG. 2.— Evolution of central temperature and density during collapse and explosion. In the final 10,000 seconds they reach maximum values of  $360$  g cm $^{-3}$  and  $8.26 \times 10^8$  K, respectively, before dropping rapidly.

instabilities now arise in the core during the explosion. Helium burning creates pressure gradients that are opposite to the gradients of density and mass fraction, which in turn gives rise to Rayleigh-Taylor instabilities. These instabilities are more violent than those in non-reactive flows because they mix the fuel with hot ash that then quickly burns the fuel, which in turn enhances the pressure gradient and drives more mixing. This explosion released  $8.82 \times 10^{54}$  erg, slightly more than in the 1D model because of the additional burning due to mixing.

Burning continues until the shock reaches the hydrogen envelope. Table 1 shows elemental abundances before and after the explosion. Energy release in this SN is primarily due to the burning of helium, oxygen and neon, which consumes  $757 M_\odot$ ,  $1116 M_\odot$ , and  $291 M_\odot$ , respectively. Burning in turn yields  $1195 M_\odot$  of  $^{24}\text{Mg}$  and  $970 M_\odot$  of  $^{28}\text{Si}$ . Few isotopes beyond  $^{28}\text{Si}$  are synthesized, with  $\ll 1 M_\odot$  of  $^{56}\text{Ni}$  being formed, not enough to be detected. Since the hydrogen envelope of the SMS is not as extended as in red supergiants, the shock does not plow up much mass when it crashes into it. The reverse shock is therefore weak and does not drive further

mixing. We show the degree to which  $^{16}\text{O}$ ,  $^{24}\text{Mg}$ ,  $^{28}\text{Si}$ , &  $^{32}\text{S}$  have mixed by the time the shock has broken out of the surface in Figure 4. Most mixing has now ceased. The major drivers of mixing in this model are fluid instabilities that emerge during burning. Mixing can cause heavy elements to be dredged up from deeper layers and appear in the SN spectra at early times.

In KEPLER models that exclude GR, the 55,500  $M_{\odot}$  star collapses to a BH instead of exploding. Likewise, if the star is 56,000  $M_{\odot}$  it collapses to a BH, even when GR is included. This suggests that there is a narrow window in mass around 55,500  $M_{\odot}$  for the progenitor masses of general relativistic supernovae (GSNe). More masses need to be tested, and more extensive nuclear reaction networks may be needed to capture all the nucleosynthetic pathways in GSNe. Our KEPLER and CASTRO simulations show that GSNe are only weakly dependent on dimensionality.

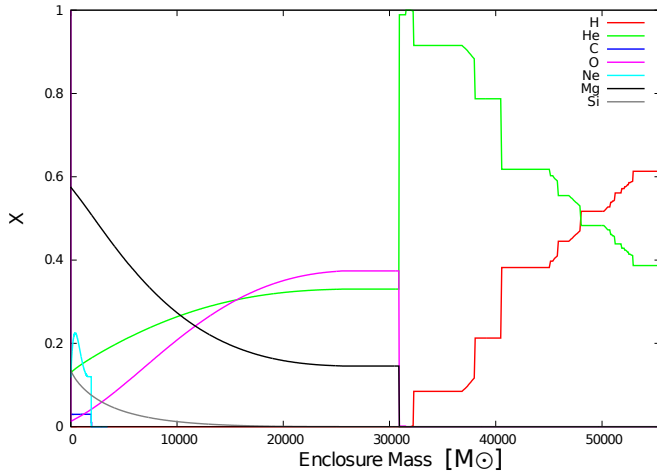


FIG. 3.— Elemental masses at the beginning of the CASTRO simulation. The mass of the helium core was about 31,000  $M_{\odot}$ . Helium abundances at the center of the star are fairly large, which implies that central helium burning is still in progress when the star collapses. Hydrogen shell burning is also still going on at the base of the envelope of the star.

Isotope	$^1\text{H}$	$^4\text{He}$	$^{12}\text{C}$	$^{16}\text{O}$	$^{20}\text{Ne}$	$^{24}\text{Mg}$	$^{28}\text{Si}$	Total
Before	$M_{\odot}$	$M_{\odot}$	$M_{\odot}$	$M_{\odot}$	$M_{\odot}$	$M_{\odot}$	$M_{\odot}$	$M_{\odot}$
After	8336	24902	922	7972	5110	7748	515	55505
$\Delta M$	-1	-757	-3	-1116	-291	1195	970	-3

TABLE 1  
ELEMENTAL MASSES BEFORE AND AFTER THE EXPLOSION.

NOTE. — The loss of 3  $M_{\odot}$  in total is due to the diffusion of the stellar envelope out of the simulation domain, which is only a tiny fraction of overall mass. It does not affect the explosion and nucleosynthesis.

GSNe are different from pair-instability SNe (PSNe; Heger & Woosley 2002; Scannapieco et al. 2005; Joggerst & Whalen 2011; Chen et al. 2011) in every aspect: what triggers the collapse, what drives the explosion, the degree of mixing, and  $^{56}\text{Ni}$  production. We compare prop-

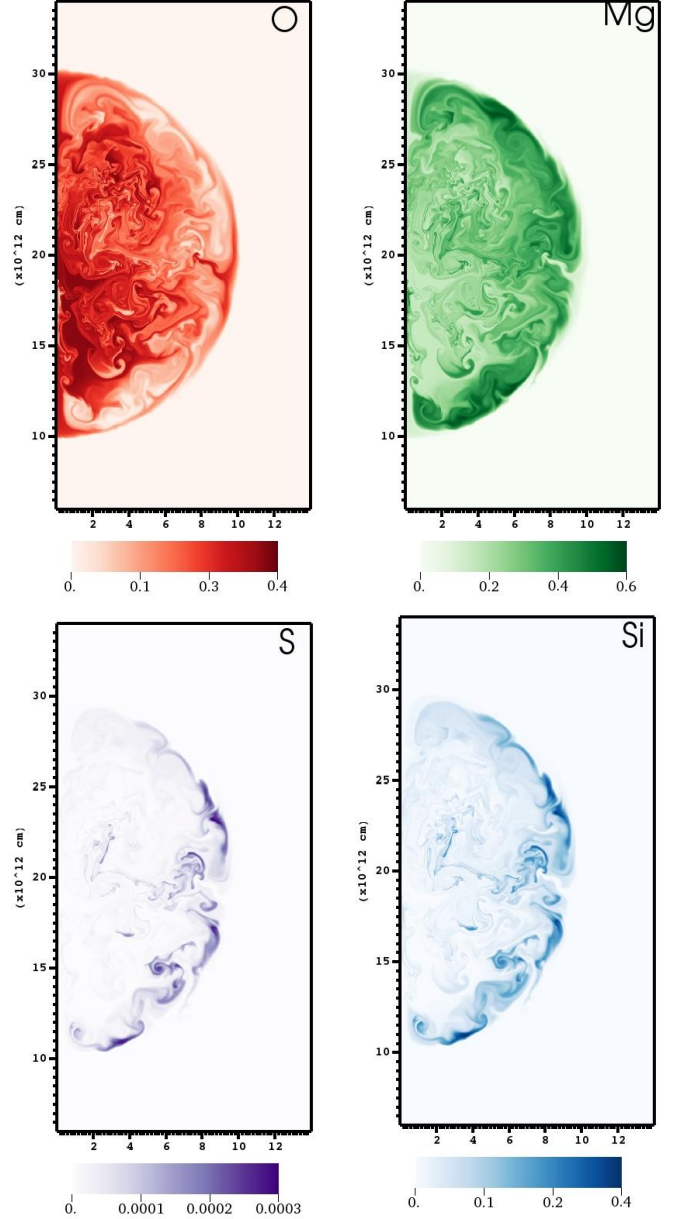


FIG. 4.— Mixing in  $^{16}\text{O}$ ,  $^{24}\text{Mg}$ ,  $^{28}\text{Si}$ , &  $^{32}\text{S}$  prior to shock breakout. Mixing on these scales might be manifest in the spectra of the explosion. Few isotopes with atomic numbers larger than  $^{28}\text{Si}$ , such as  $^{32}\text{S}$ , are formed.

erties of PSNe and GSNe in Table 2. In GSNe, only a trace amount of  $^{56}\text{Ni}$  ( $\ll 1 M_{\odot}$ ) is produced at the edge of the oxygen-burning shell by  $\alpha$  capture. PSNe can synthesize up to 50  $M_{\odot}$  of  $^{56}\text{Ni}$  through explosive  $^{28}\text{Si}$  burning. The light curves of GSNe are mainly powered by the thermal emission by hot ejecta and the conversion of kinetic energy into entropy by the shock, not  $^{56}\text{Ni}$  decay. Large masses of elements with atomic masses between  $^{12}\text{C}$  and  $^{28}\text{Si}$  are synthesized during the explosion, and they are all dispersed into the surrounding medium.

## 5. DISCUSSION AND CONCLUSION

We have discovered that Pop III stars with masses of 55,500  $M_{\odot}$  may explode as SNe instead of collapsing to BHs. GR effects, rather than the pair instability, trig-

Characteristic Property	PSNe	GSNe
Progenitor Mass ( $M_{\odot}$ )	150 – 260	$\sim 55, 500$
Collapse Trigger	Pair Instability	GR Instability
Explosive Burning	$^{16}\text{O}$ , $^{28}\text{Si}$	$^4\text{He}$
$^{56}\text{Ni}$ Production ( $M_{\odot}$ )	0.1 – 50	$\ll 1$
Explosion Energy (erg)	$1 - 100 \times 10^{51}$	$6 - 9 \times 10^{54}$
Fluid Instabilities	Reverse Shock	Burning

TABLE 2  
COMPARISON BETWEEN PSNe AND GSNe

ger the explosion, which at  $\sim 9 \times 10^{54}$  erg is the most energetic thermonuclear SN known. Mixing in 2D enhances burning and thermonuclear yields during the explosion, which completely unbinds the star and leaves no compact remnant. Energy release is primarily due to explosive helium burning after the onset of central helium burning. The explosion yields mostly elements between carbon and silicon, with almost no iron group elements. Besides enhancing burning, mixing during the SN can dredge up heavy elements from deeper layers and cause them to appear at earlier times in spectra.

Our simulations are approximate for several reasons. First, we do not model the evolution of the protostar from much lower masses. Instead, the star is initialized at the beginning of the main sequence in *KEPLER*. Next, we did not evolve the star under the heavy ongoing accretion that gave birth to the star. We also did not consider stellar rotation, which could lower the mass at which the star explodes (e.g., Chatzopoulos & Wheeler 2012; Chatzopoulos et al. 2013). There is growing evidence that many Pop III stars are born with high rates of spin (Stacy et al. 2011; Greif et al. 2012). Finally, we did not include UV feedback from the star, which could regulate its accretion rates. However, in some cases luminosity from the star is thought to terminate accretion (Johnson et al. 2012), so our assumption that the star has a constant mass is plausible. Efforts are now underway to survey Pop III protostellar evolution under a variety of accretion rates and SMS evolution with much larger and finer grids in mass.

What effect would such an explosion have on the protogalaxy that gave birth to the star? The answer depends on the ambient density of the SN. If the SMS grows by accretion through a disk its UV radiation will break free of the disk and ionize the surrounding envelope. In these circumstances the star would explode in low densities, and Johnson et al. (2013b) show that the SN would drive all the gas from the protogalaxy, perhaps engulfing nearby protogalaxies with metals. Much of this material would later fall back to the halo on timescales of 50 - 100 Myr and form stars. If accretion is spherical, then

the star will not ionize its envelope and it will explode in very high densities (Johnson et al. 2012; Hosokawa et al. 2013; Schleicher et al. 2013). In this scenario, Whalen et al. (2013a,b) find that much of the energy of the explosion is promptly radiated away by bremsstrahlung X-rays and inverse Compton scattering of cosmic microwave background (CMB) photons, but that the SN remnant still expands to roughly the virial radius of the halo,  $\sim 1$  kpc, and then collapses back into the halo. Collapse thoroughly mixes baryons in the halo with metals and may trigger a starburst that would easily distinguish this protogalaxy from its dimmer and less rapidly evolving neighbors.

Radiation hydrodynamical simulations show that the GSN would be visible at  $z \lesssim 20$  to future all-sky NIR surveys by *Euclid*, the Wide-Field Infrared Survey Telescope (WFIRST) and the Wide-field Imaging Surveyor for High-Redshift (WISH) (Whalen et al. 2013c). The wide survey fields and high sensitivities of these missions would enable them to detect such an event anywhere in the universe, even if their numbers are small. Furthermore, a single GSN can create 100 times the chemical yield of a PSN. But unlike PSNe, which synthesize more iron group elements, GSNe would mainly enrich primordial gas with elements from  $^{12}\text{C}$  to  $^{28}\text{Si}$ . Traces of GSNe might therefore be found in early galaxies that are  $^{56}\text{Fe}$  deficient but enhanced with  $^{12}\text{C}$  and  $^{16}\text{O}$  (Keller et al. 2014). Whether in future NIR campaigns or in the fossil abundance record, the detection of GSNe in the early universe may soon signal the birth of SMBH seeds and the first quasars.

The authors thank the members of CCSE at LBNL for help with *CASTRO*. We also thank Volker Bromm, Dan Kasen, Lars Bildsten, John Bell, and Adam Burrows for many useful discussions. K.C. was supported by an IAU-Gruber Fellowship, a Stanwood Johnston Fellowship, and a KITP Graduate Fellowship. A.H. was supported by a Future Fellowship from the Australian Research Council (ARC FT 120100363). D.J.W. was supported by the Baden-Württemberg-Stiftung by contract research under the programme Internationale Spitzenforschung II (grant P-LS-SPII/18). All numerical simulations were performed at the University of Minnesota Supercomputing Institute and the National Energy Research Scientific Computing Center. This work was supported by the DOE grants de-sc0010676, DE-AC02-05CH11231, DE-GF02-87ER40328, DE-FC02-09ER41618 and by NSF grants AST-1109394 and PHY02-16783. Work at LANL was done under the auspices of the National Nuclear Security Administration of the US Department of Energy at Los Alamos National Laboratory under Contract No. DE-AC52-06NA25396.

## REFERENCES

- Agarwal, B., Khochfar, S., Johnson, J. L., Neistein, E., Dalla Vecchia, C., & Livio, M. 2012, *MNRAS*, 425, 2854  
 Almgren, A. S., et al. 2010, *ApJ*, 715, 1221  
 Alvarez, M. A., Wise, J. H., & Abel, T. 2009, *ApJ*, 701, L133  
 Baraffe, I., Heger, A., & Woosley, S. E. 2001, *ApJ*, 550, 890  
 Baumgarte, T. W., & Shapiro, S. L. 1999, *ApJ*, 526, 941  
 Begelman, M. C. 2010, *MNRAS*, 402, 673  
 Begelman, M. C., Volonteri, M., & Rees, M. J. 2006, *MNRAS*, 370, 289  
 Beifiori, A., Courteau, S., Corsini, E. M., & Zhu, Y. 2012, *MNRAS*, 419, 2497  
 Bisnovatyi-Kogan, G. S. 1998, *ApJ*, 497, 559  
 Bond, J. R., Arnett, W. D., & Carr, B. J. 1984, *ApJ*, 280, 825  
 Bromm, V., & Loeb, A. 2003, *ApJ*, 596, 34  
 Bromm, V., & Yoshida, N. 2011, *ARA&A*, 49, 373  
 Carr, B. J., Bond, J. R., & Arnett, W. D. 1984, *ApJ*, 277, 445  
 Chandrasekhar, S. 1939, An introduction to the study of stellar structure

- Chatzopoulos, E., & Wheeler, J. C. 2012, *ApJ*, 748, 42
- Chatzopoulos, E., Wheeler, J. C., & Couch, S. M. 2013, *ApJ*, 776, 129
- Chen, K., Heger, A., & Almgren, A. S. 2011, *Computer Physics Communications*, 182, 254
- Chen, K.-J., Heger, A., & Almgren, A. S. 2013, *Astronomy and Computing*, 34, 70
- Di Matteo, T., Springel, V., & Hernquist, L. 2005, *Nature*, 433, 604
- Ekström, S., Meynet, G., Chiappini, C., Hirschi, R., & Maeder, A. 2008, *A&A*, 489, 685
- Fan, X., Narayanan, V. K., Strauss, M. A., White, R. L., Becker, R. H., Pentericci, L., & Rix, H.-W. 2002, *AJ*, 123, 1247
- Fan, X., et al. 2006, *AJ*, 132, 117
- Ferrarese, L., & Ford, H. 2005, *Space Sci. Rev.*, 116, 523
- Ferrarese, L., & Merritt, D. 2000, *ApJ*, 539, L9
- Fowler, W. A. 1966, *ApJ*, 144, 180
- Fuller, G. M., Woosley, S. E., & Weaver, T. A. 1986, *ApJ*, 307, 675
- Gebhardt, K., et al. 2000, *ApJ*, 539, L13
- Greif, T. H., Bromm, V., Clark, P. C., Glover, S. C. O., Smith, R. J., Klessen, R. S., Yoshida, N., & Springel, V. 2012, *MNRAS*, 424, 399
- Heger, A., & Woosley, S. E. 2002, *ApJ*, 567, 532
- Heger, A., Woosley, S. E., Martínez-Pinedo, G., & Langanke, K. 2001, *ApJ*, 560, 307
- Hosokawa, T., Yorke, H. W., Inayoshi, K., Omukai, K., & Yoshida, N. 2013, *ApJ*, 778, 178
- Joggerst, C. C., & Whalen, D. J. 2011, *ApJ*, 728, 129
- Johnson, J. L., & Bromm, V. 2007, *MNRAS*, 374, 1557
- Johnson, J. L., Dalla, V. C., & Khochfar, S. 2013a, *MNRAS*, 428, 1857
- Johnson, J. L., Whalen, D. J., Even, W., Fryer, C. L., Heger, A., Smidt, J., & Chen, K.-J. 2013b, *ApJ*, 775, 107
- Johnson, J. L., Whalen, D. J., Fryer, C. L., & Li, H. 2012, *ApJ*, 750, 66
- Johnson, J. L., Whalen, D. J., Li, H., & Holz, D. E. 2013c, *ApJ*, 771, 116
- Karlsson, T., Bromm, V., & Bland-Hawthorn, J. 2013, *Reviews of Modern Physics*, 85, 809
- Keller, S. C., et al. 2014, *ArXiv e-prints*
- Kippenhahn, R., & Weigert, A. 1990, *Stellar Structure and Evolution*
- Kormendy, J., & Richstone, D. 1995, *ARA&A*, 33, 581
- Krtićka, J., & Kubát, J. 2006, *A&A*, 446, 1039
- Kudritzki, R. 2000, in *The First Stars*, ed. A. Weiss, T. G. Abel, & V. Hill, 127–+
- Latif, M. A., Schleicher, D. R. G., Schmidt, W., & Niemeyer, J. 2013a, *MNRAS*, 433, 1607
- . 2013b, *MNRAS*, 430, 588
- Lodato, G., & Natarajan, P. 2006, *MNRAS*, 371, 1813
- Loeb, A., & Rasio, F. A. 1994, *ApJ*, 432, 52
- Madau, P., & Rees, M. J. 2001, *ApJ*, 551, L27
- McConnell, N. J., & Ma, C.-P. 2013, *ApJ*, 764, 184
- Montero, P. J., Janka, H.-T., & Müller, E. 2012, *ApJ*, 749, 37
- Mortlock, D. J., et al. 2011, *Nature*, 474, 616
- Park, K., & Ricotti, M. 2011, *ApJ*, 739, 2
- . 2012, *ApJ*, 747, 9
- . 2013, *ApJ*, 767, 163
- Rees, M. J. 1984, *ARA&A*, 22, 471
- Regan, J. A., & Haehnelt, M. G. 2009, *MNRAS*, 396, 343
- Reisswig, C., Ott, C. D., Abdikamalov, E., Haas, R., Moesta, P., & Schnetter, E. 2013, *arXiv:1304.7787*
- Scannapieco, E., Madau, P., Woosley, S., Heger, A., & Ferrara, A. 2005, *ApJ*, 633, 1031
- Schleicher, D. R. G., Palla, F., Ferrara, A., Galli, D., & Latif, M. 2013, *A&A*, 558, A59
- Shang, C., Bryan, G. L., & Haiman, Z. 2010, *MNRAS*, 402, 1249
- Shapiro, S. L., & Teukolsky, S. A. 1979, *ApJ*, 234, L177
- Shibata, M., & Shapiro, S. L. 2002, *ApJ*, 572, L39
- Spaans, M., & Silk, J. 2006, *ApJ*, 652, 902
- Stacy, A., Bromm, V., & Loeb, A. 2011, *MNRAS*, 413, 543
- Timmes, F. X. 1999, *ApJS*, 124, 241
- Timmes, F. X., & Swesty, F. D. 2000, *ApJS*, 126, 501
- Vink, J. S., de Koter, A., & Lamers, H. J. G. L. M. 2001, *A&A*, 369, 574
- Volonteri, M. 2010, *A&A Rev.*, 18, 279
- . 2012, *Science*, 337, 544
- Weaver, T. A., Zimmerman, G. B., & Woosley, S. E. 1978, *ApJ*, 225, 1021
- Whalen, D., Abel, T., & Norman, M. L. 2004, *ApJ*, 610, 14
- Whalen, D. J., & Fryer, C. L. 2012, *ApJ*, 756, L19
- Whalen, D. J., Johnson, J. L., Smidt, J., Heger, A., Even, W., & Fryer, C. L. 2013a, *ApJ*, 777, 99
- Whalen, D. J., Johnson, J. L., Smidt, J., Meiksin, A., Heger, A., Even, W., & Fryer, C. L. 2013b, *ApJ*, 774, 64
- Whalen, D. J., et al. 2013c, *ApJ*, 778, 17
- Wheeler, J. C. 1977, *Ap&SS*, 50, 125
- Wise, J. H., Turk, M. J., & Abel, T. 2008, *ApJ*, 682, 745
- Zeldovich, Y. B., & Novikov, I. D. 1971, *Relativistic astrophysics. Vol.1: Stars and relativity*
- Zhang, W., Howell, L., Almgren, A., Burrows, A., & Bell, J. 2011, *ApJS*, 196, 20